PROCEEDINGS, 50th Workshop on Geothermal Reservoir Engineering
Stanford University, Stanford, California, February 10-12, 2025
SGP-TR-229

Modeling Near-Wellbore Tortuosity at Utah FORGE Site

Wei Fu[1*], Branko Damjanac[1], Zorica Radakovic-Guzina[1], Robert Podgorney[2], John Mclennan[3]

1 Itasca Consulting Group, Inc., Minneapolis, MN, USA

2 Idaho National Laboratory, Idaho Falls, ID, USA

3 Department of Chemical Engineering, University of Utah, Salt Lake City, UT, USA

* wei@itascacg.com

Keywords: Near-Wellbore Tortuosity, Cement Sheath, Perforation, Enhanced Geothermal System (EGS), Thermo-Hydro-Mechanical Modeling, Wellbore Cooling

ABSTRACT

Near-wellbore tortuosity directly influences the flow efficiency between the wellbore and the rock matrix. The tortuosity-induced pressure drop elevates the injection pressure required for reservoir stimulation, as well as increasing the fluid circulation pressure during production, leading to high long-term energy consumption and operational costs. In this paper, we present a three-dimensional thermo-hydro-mechanical numerical model to investigate the hydraulic fracture propagation in the near-wellbore region. The study is based on the Stage 4 stimulation of Well 16A(78)-32 at the Utah FORGE site completed in 2024, which used a case-hole approach and slickwater as the fracturing fluid. The model takes a discrete element modeling approach and explicitly represents the well casing, cement sheath, and 36 perforation tunnels. This enables a detailed representation of the complex stress field resulting from the combined effects of subsurface in-situ stresses and stress concentrations around the wellbore and perforations. Furthermore, the model simulates the cooling effect on the stress field in the near-wellbore region, accounting for thermal responses within the casing-cement-perforation-rock structure. The simulation results highlight complex near-wellbore fracture growth phases, including fracture initiation, merging, longitudinal fracture growth, and transverse fracture growth. The predicted early-time bottomhole pressure from the simulation shows reasonable agreement with the field data within an acceptable range of deviation.

1. INTRODUCTION

FORGE is a U.S. Department of Energy funded project with the objectives of developing and testing techniques for creating, sustaining, and monitoring Enhanced Geothermal System (EGS) reservoirs (McLennan et al. 2023). In April of 2024, seven stimulation stages were performed from the injection well 16A(78)-32 with plug and perf completions using different injection fluids, cluster spacings, and cluster counts. In the fracturing stages performed at FORGE, including the treatments conducted in 2022, bottomhole pressure much higher than the minimum principal stress has been observed. The net pressure in the early time of these stages exceeds 20 MPa, which is greater than typical fracturing pressures. This suggests significant near-wellbore tortuosity. The study of 62 diagnostic fracture injection tests in shale by McClure et al (2022) shows that near-wellbore pressure drops in horizontal wells can be thousands of psi (tens of MPa). In the context of enhanced geothermal systems, fracture behavior in the near-wellbore region is more complex due to the cooling effect of the injection fluid, which induces thermal and mechanical effects within the casing-cement-perforation-rock structure.

Near-wellbore tortuosity directly influences the flow efficiency between the wellbore and the rock matrix. For reservoir stimulation, it elevates the injection pressure required for fracture propagation, which could exceed operational constraints. Complex fracture geometries in the near-wellbore region can cause localized proppant bridging, potentially leading to wellbore screen-out. Near-wellbore tortuosity will also increase the fluid circulation pressure during production due to increased resistance to fluid flow out of and into the wells. During the nine-hour circulation tests between wells 16A(78)-32 and 16B(78)-32 in April 2024 and the extended circulation in August 2024, the surface injection pressure was around 3000 psi (~20 MPa), which needs to be adequately reduced to improve the long-term operational costs for large-scale commercial applications.

In this study, we developed a wellbore model using a distinct element method, which explicitly incorporates well casing, cement sheath, and perforation tunnels, alongside the reservoir rock. The model simulates the cooling effect on the stress field in the near-wellbore region, accounting for thermal responses within the casing-cement-perforation-rock structure. At the perforation level, the model uses millimeter-scale resolution, consistent with the grain and microcrack length scales in rock, enabling proper simulation of fracture initiation around perforation tunnels.

2. ENGINEERING BACKGROUND

At the Utah FORGE site, injection well 16A(78)-32 was drilled at a 65° inclination angle from vertical. A three-stage fracturing treatment was initially performed at the toe of the well in 2022, followed by seven additional stimulation stages in 2024. The focus of this study is Stage 4 of Well 16A(78)-32, completed in 2024, which has a true vertical depth of 8205 ft (2500 m), as shown in Figure 1. During this stage, slickwater was pumped down the casing at a rate of 10 bpm (0.0265 m^3/s) until breakdown happened. The stage includes a single

6-foot perforation cluster with six shots per foot at 60° phasing, resulting in a total of 36 perforations in the well casing. The minimum principal stress is oriented horizontally, which favors hydraulic fracture growth in the vertical direction.

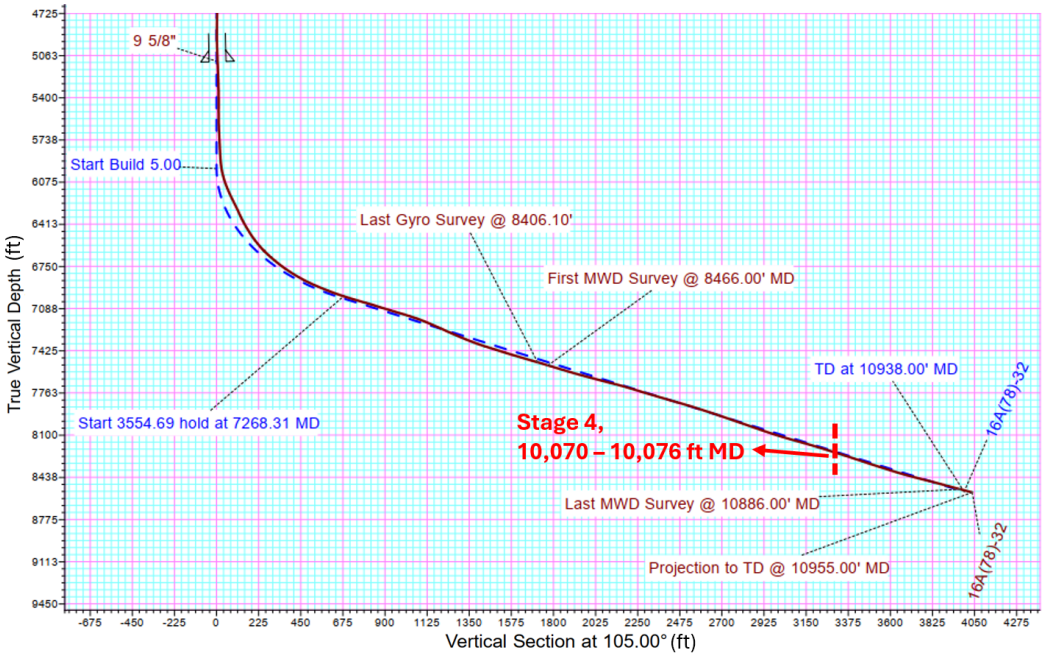

Figure 1: Trajectory of well 16A(78)-32 in a vertical cross-section at the Utah FORGE site and the location of Stage 4, at TVD of 8205 ft.

3. NUMERICAL SIMULATION

3.1 Numerical Model

The simulations of fluid injections and hydraulic fracturing within the rock mass were conducted using the XSite numerical code, a DEM code that employs the synthetic rock mass (SRM) method with a lattice numerical approach. Detailed verifications of hydraulic fracture propagation across various regimes have been performed, as demonstrated by Damjanac & Cundall (2016) for the viscosity-dominated regime and Fu et al. (2019) for the toughness-dominated regime. Thermal mechanisms have been incorporated in the code to model heat advection through the fracture fluid, forced heat convection at the rock-fluid interface, and heat conduction within the rock, coupled with overall mechanical deformation (Detournay et al., 2022).

3.2 Numerical Model Setup

The dimensions of the model are 6 m × 6 m × 6 m (L × W × H). A 4-m long section of the wellbore is placed vertically in local coordinates in the center of the simulation domain, with a 1.8-m long (6 ft) perforated section in the middle of the wellbore. The well casing, cement sheath, and perforation tunnels are explicitly represented, as shown in Figure 2. The in-situ stress conditions were implemented such that the orientation of the wellbore relative to the principal stresses is the same as in the field. A total of 36 perforations phased at 60° were simulated, with 6 shots per foot density, consistent with the design of Stage 4. The far-field boundaries of the model are fixed, and the magnitudes of the in-situ stresses, shown in Table 1, are chosen to be the same as the in-situ stresses for Stage 4.

The impact of discrete fracture networks (DFN) has been explored in previous modeling efforts for Stage 2 at FORGE, which demonstrated that natural fractures intersecting perforation tunnels at a favorable angle relative to in-situ stress directions can enhance fracture initiation in hard rocks (Fu et al., 2024). Stage 2 features a 20-ft long perforation interval with 120 perforations, aiming to increase the likelihood of intersecting natural fractures identified through wellbore image log analysis (McLennan et al. 2023). In contrast, Stage 4 has a much shorter perforation cluster length and fewer perforations, and a DFN is not included in this model.

The granite rock is assumed to have a temperature of 219 °C. Field operations before the stimulation stages, such as cold fluid injection and wellbore pressure test, led to cooling and heating cycles of the casing-cement-perforation-rock structure. To account for these effects, we assume a 100 °C difference between the wellbore wall and the rock matrix in the simulation.

The model was initially brought to equilibrium following the excavation of the wellbore and casing perforation after the installation of the casing and cement sheath. A fixed temperature boundary condition of 119°C was then applied to the wellbore wall for one hour of cooling. Figure 3 illustrates the temperature distribution along the wellbore after cooling, with a 100°C temperature difference between the wellbore wall and the rock. The temperature decreases progressively in the vicinity of the wellbore, indicating a significant cooling

effect. Thermal and mechanical calculations were conducted to resolve the heat transfer and thermally induced stresses in the casing, cement, and rock. Subsequently, fluid was injected into the wellbore to initiate and propagate hydraulic fractures.

The casing, cement, rock properties, fluid properties, and in-situ stress magnitudes are summarized in Table 1.

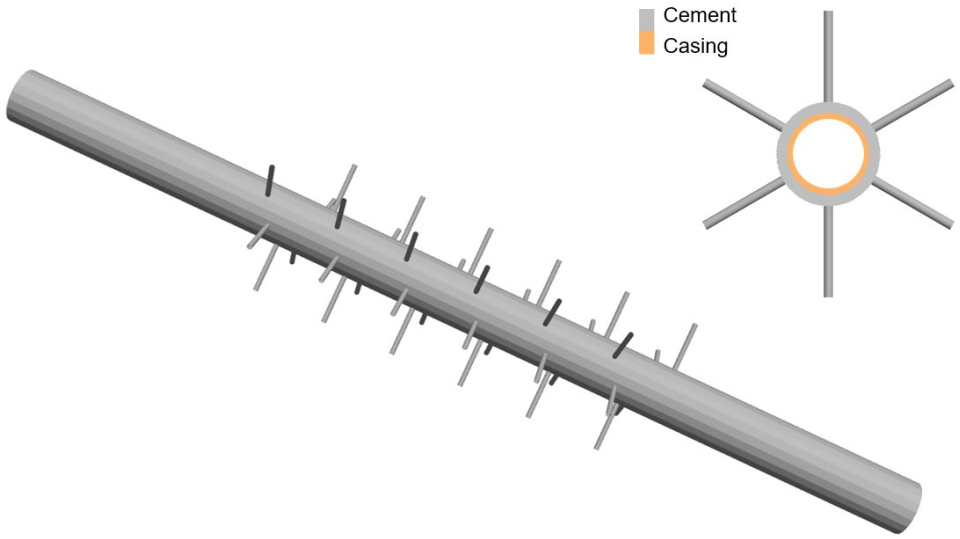

Figure 2: Perforated wellbore and the transverse cross-section displaying the 60-degree phasing perforation tunnels, steel casing, and cement sheath.

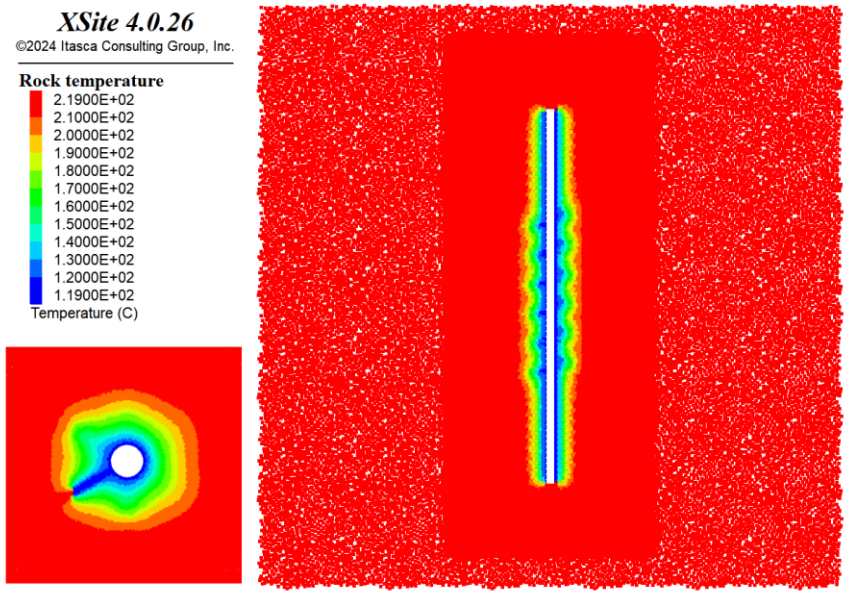

Figure 3: Temperature field around the wellbore after one hour of cooling, a temperature difference of 100 °C was assumed between the wellbore wall and the far-field rock matrix.

Table 1 Input parameters for the near-wellbore model, well 16A(78)-32, Stage 4.

Parameters	Granite	Cement	Casing
Young's modulus, GPa	55	20.7	200
Poisson's ratio	0.26	0.17	0.28
Fracture toughness, MPa×m$^{1/2}$	3	1	/
Thermal Conductivity (W/m*°C)	3.0	1.7	15.0
Thermal Expansion Coefficient (1/°C)	6.0e-6	1.0e-5	1.3e-5
Fluid viscosity, cp	2		
Pore pressure, MPa	23.26 (3400 psi)		
Minimum horizontal stress, MPa	41.27 (6000 psi)		
Maximum horizontal stress, MPa	47.27 (6900 psi)		
Vertical stress, MPa	60.77 (8800 psi)		

4. RESULTS AND DISCUSSION

4.1 Injection Pressure

The near-wellbore tortuosity effect is important for numerical simulations to properly capture the pressure responses during hydraulic fracturing. This has been challenging due to complex influencing factors across scales that need to be considered by a model. Field-scale simulations typically assume an empirical pressure drop in order to account for the tortuosity and match the pressure history data (McClure et al. 2023, Lee and Ghassemi, 2024).

Figure 4 shows the injection pressure history for Stage 4 of well 16A(78)-32 (Energy and Geoscience Institute at the University of Utah, 2024). The peak bottom hole pressure approaches 10,000 psi. While the sustained high fluid pressure after breakdown pressure is partly attributed to the ramping-up of the injection rate, a high propagation pressure of approximately 8,000 psi is maintained during fracture propagation. This corresponds to a net pressure of around 2,000 psi, indicating significant frictional effects and associated pressure drops.

Figure 5 shows the bottomhole pressure history obtained from the near-wellbore model, focusing on the early-time behavior. Injection begins at a simulation time of 3601 s and lasts for approximately 3 s. After a brief period of steady pressure increase, the bottomhole pressure peaks at 71 MPa, followed by a gradual decline, though it remains at a relatively high level. These pressure responses suggest a complex fracture trajectory in the near-wellbore region, preventing the sharp pressure drop typically expected during single fracture growth. In Figure 5, we calculated the upper bound (blue dashed line) of the breakdown pressure by summing the recorded peak surface pressure and the hydrostatic pressure corresponding to the true vertical depth (TVD) of Stage 4, without accounting for any pressure drops; the lower bound is taken from the peak bottomhole pressure in Fig. 2, defining a range of ~ 68 MPa – 75 MPa. Considering uncertainties associated with pressure recording and pressure drop estimations, the predicted early-time bottomhole pressure by the simulation shows reasonable agreement with the field data.

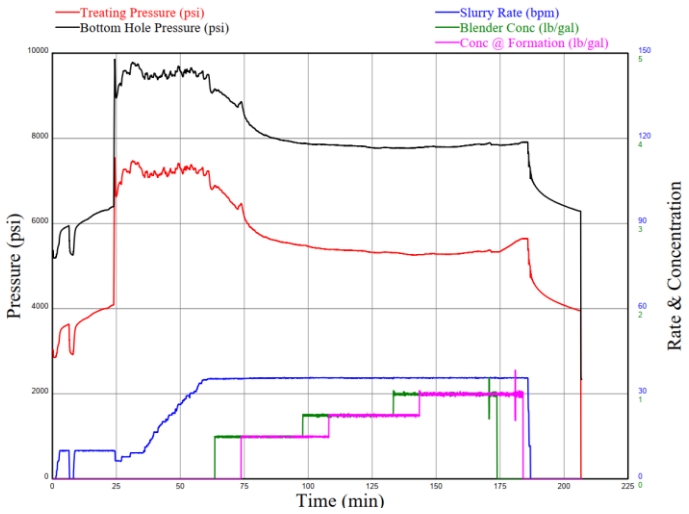

Figure 4: Injection pressure history for Stage 4 of well 16A(78)-32, the peak bottomhole pressure is close to 10,000 psi (69 MPa) (Energy and Geoscience Institute at the University of Utah, 2024).

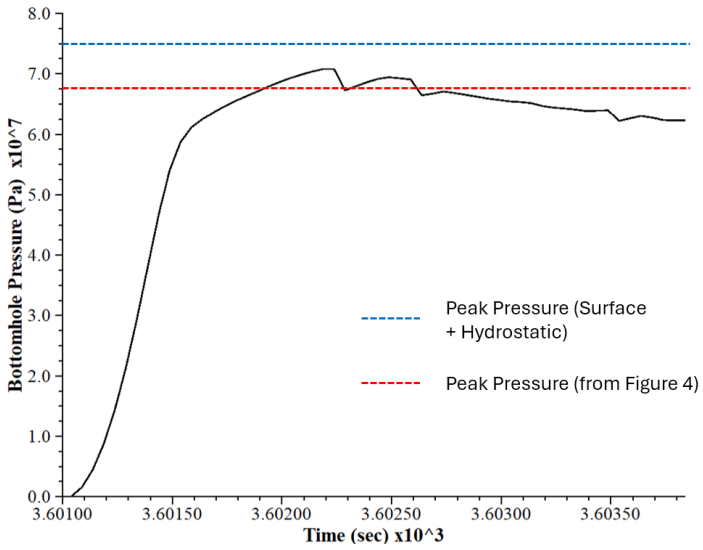

Figure 5: Bottomhole pressure history. Fluid injection started at 3601 s. The upper bound is obtained by summing the recorded peak surface pressure and hydrostatic pressure corresponding to the TVD of Stage 4; the lower bound is taken from the peak bottomhole pressure in Fig. 2.

4.2 Near-wellbore Tortuosity

Fracture Initiation

The evolution of hydraulic fracture initiation and growth near the wellbore is shown in Figure 6. At an early injection time (t = 0.8 s), fractures accumulate around both the wellbore and the perforation tunnels. While fracture initiation from the perforation tunnels is anticipated, the cross-sectional plot shows that fractures also extend into the cement, along the cement-rock boundaries, and into the rock near the cement. Two primary factors contribute to this behavior. The cement has lower strength, making it prone to tensile failure and hydraulic fracture growth into the cemented region. In addition, the cooling effect further reduces compressive stress within the rock and cement near the wellbore, potentially leading to tensile conditions. This change in stress state further promotes fracture initiation around the wellbore.

Fracture Merging and Longitudinal Growth

Following initiation, the fractures continue to grow, and significant tortuosity is formed along the wellbore (Figure 7), characterized by fracture twisting, merging, and growing in different directions. Despite limited fracture growth in the plane of the minimum in-situ stress (plan view, left subplot), the microcracks generated by fluid injection through different perforation tunnels merge into larger fractures, predominantly growing in the longitudinal direction along the well. These fractures primarily develop in the plane of the maximum horizontal stress, suggesting that the near-wellbore stress field exerts a greater influence on fracture trajectories than the far-field stress state. Such longitudinal growth is further favored particularly after fractures have already formed around the wellbore during the initial phase, due to combined effects of cooling, cement bonding state, and in-situ stress conditions.

Fracture Transverse Growth

At the early time of fluid injection, fractures primarily propagate along the wellbore (Figures 8a, 8b). As injection continues, longitudinal growth begins to slow down. As shown by the change in fracture trajectory in Figures 8c and 8d, fractures at both ends of the perforation cluster start to curve into the plane of minimum in-situ stress, while those in the middle of the cluster become inhibited. This behavior resembles fracture propagation in a multi-cluster stage, where the outer fractures dominate due to more favorable stress conditions. Eventually, one wing of the fracture becomes dominant, continuing to propagate while curving toward the direction of minimum in-situ stress.

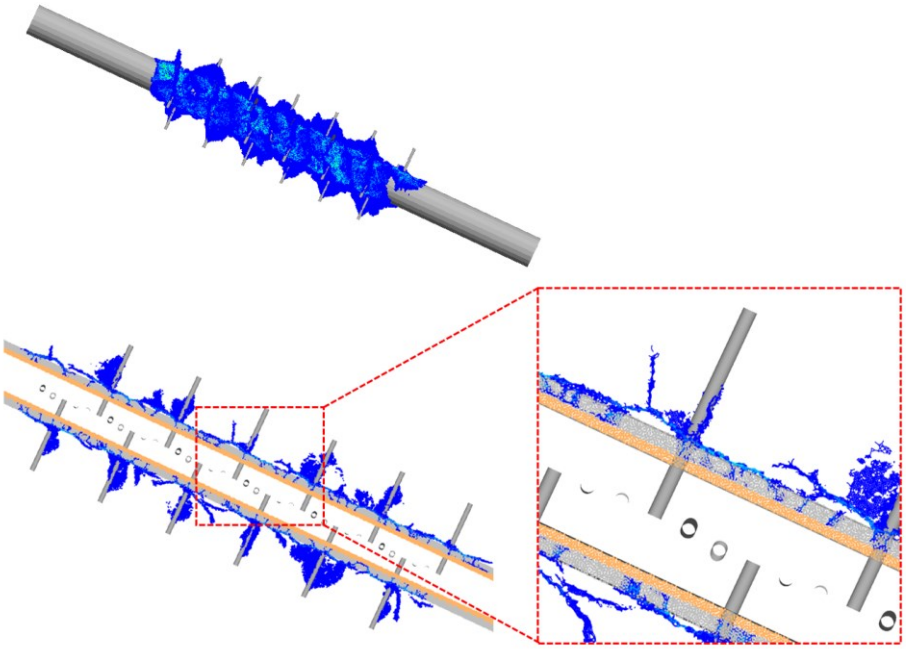

Figure 6: Fracture initiation and propagation near the wellbore at early time (t = 0.8 s).

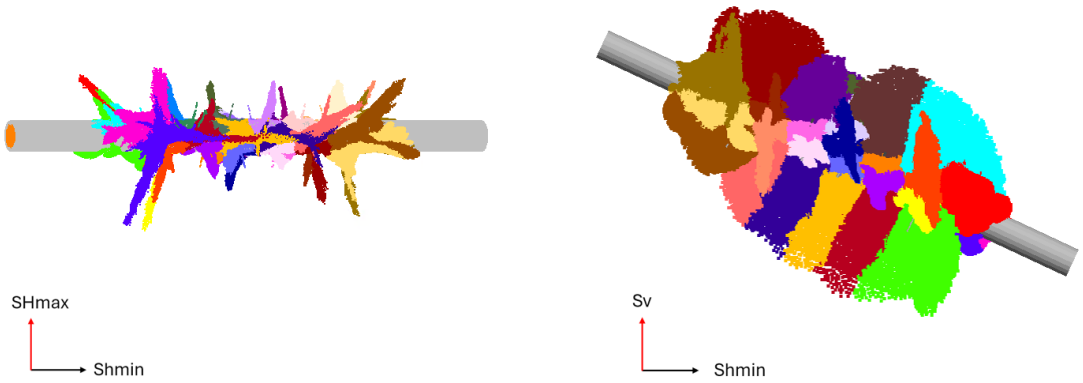

Figure 7: Continued fracture growth following initiation, with longitudinal fractures dominating the growth. The left plot presents a plan view; the right plot is oriented such that the simulated wellbore aligns consistently with the actual direction of the wellbore in situ, with the minimum principal stress in the horizontal direction. Microcracks resulting from fluid injection through different perforation tunnels are represented in different colors (t = 1.6 s).

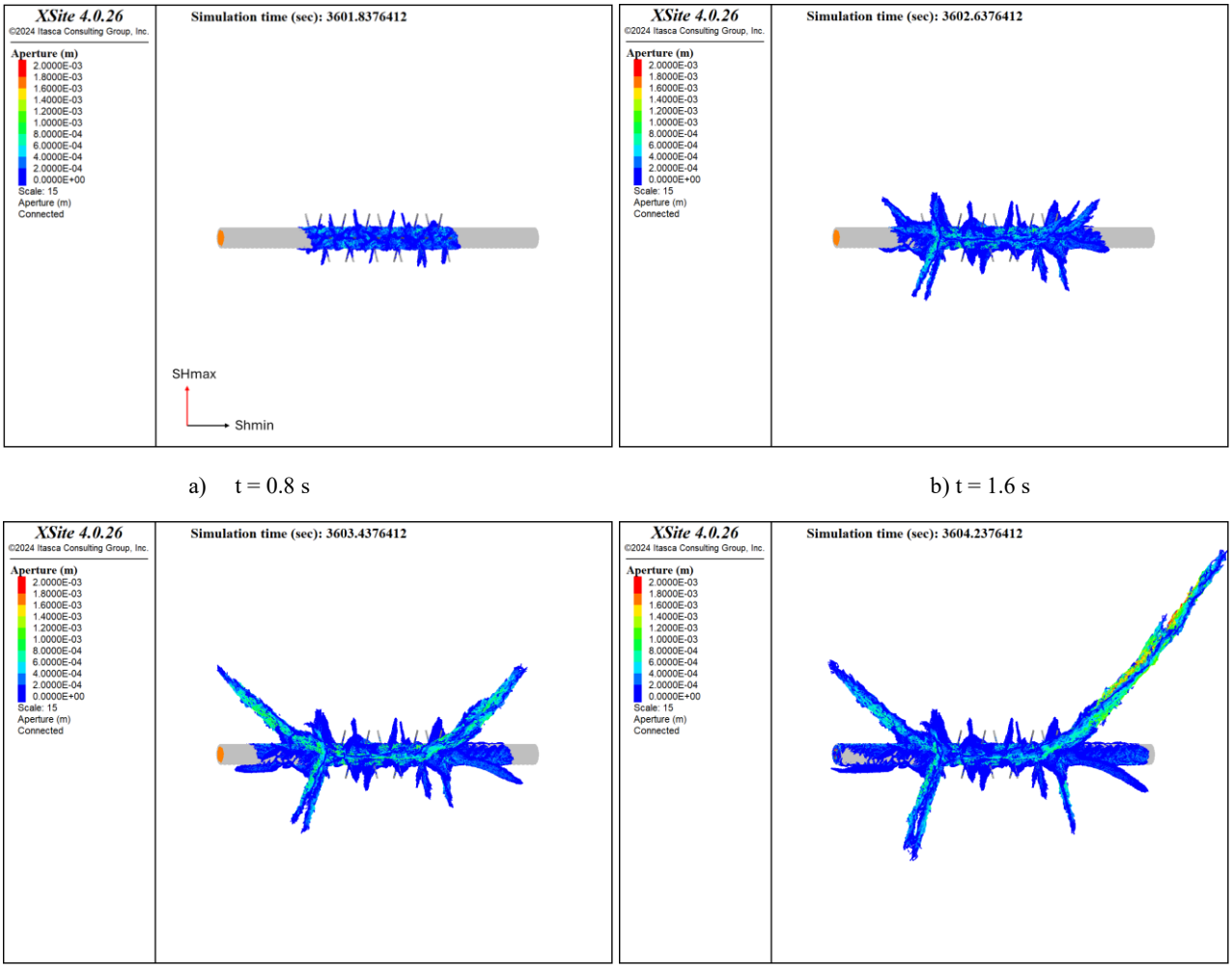

a) t = 0.8 s

b) t = 1.6 s

c) = 2.4 s

d) t = 3.2 s

Figure 8: Fracture geometry at different injection times, plan view. The simulations were stopped before the fractures reached the model boundary.

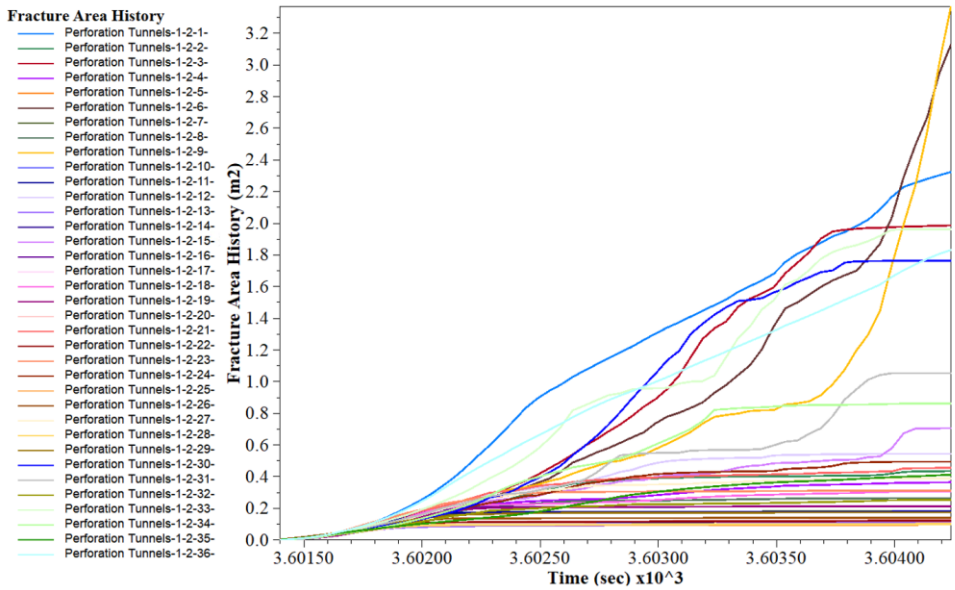

Figure 9: Fracture area resulting from fluid injection through different perforation tunnels.

4.3 Perforation Efficiency

Figure 9 illustrates the fracture area associated with different perforation tunnels, providing a measure of how effectively the perforations within the cluster facilitate fluid injection and hydraulic fracture propagation. During fracture initiation at an early time, fracture areas develop relatively uniformly across the perforations. However, by the end of the simulation, the majority of the fracture area is generated by only 7 out of 36 perforations, with 4 perforations continuing to show an increasing trend in fracture growth. This results in a low perforation efficiency of approximately 10% ~ 20%. Such low efficiency can lead to uneven fluid distribution and high perforation pressure drops.

5. CONCLUSIONS

This study presents a three-dimensional thermo-hydro-mechanical numerical simulation of near-wellbore tortuosity at Utah FORGE site. The model explicitly simulates the casing-cement-perforation-rock structure, resolves coupled hydraulic fracture propagation, and considers the wellbore cooling effect.

The simulation results highlight complex near-wellbore fracture growth mechanisms contributing to near-wellbore tortuosity, including fracture initiation, merging, longitudinal propagation, and transverse propagation. Early-time fracture propagation can happen both within the cement and rock matrix around the wellbore due to the lower strength of the cement and the cooling effect that further reduces the compressive stress in the rock. While these effects facilitate fracture initiation, their combined influence on near-wellbore tortuosity considering different cooling scenarios require further investigation.

Longitudinal fractures primarily develop in the plane of maximum horizontal stress, resulting in elevated propagation pressures before transitioning into transverse fractures over time. Furthermore, the model predicts a breakdown pressure of 71 MPa, which exhibits reasonable agreement with field data. The simulation also indicates a low perforation efficiency of approximately 10% ~ 20%, which indicates the need for further research on perforation design in geothermal applications.

ACKNOWLEDGEMENTS

Funding for this work was provided by the U.S. Department of Energy under grant DE-EE0007080 “Enhanced Geothermal System Concept Testing and Development at the Milford City, Utah FORGE Site.” We thank the many stakeholders supporting this project, including Smithfield, Utah School and Institutional Trust Lands Administration, and Beaver County, as well as the Utah Governor’s Office of Energy Development. This research made use of the resources of the High-Performance Computing Center at Idaho National Laboratory, which is supported by the Office of Nuclear Energy of the U.S. Department of Energy and the Nuclear Science User Facilities under Contract No. DE-AC07-05ID14517.

REFERENCES

Damjanac, B., & Cundall, P. (2016). Application of Distinct Element Methods to Simulation of Hydraulic Fracturing in Naturally Fractured Reservoirs. Computers and Geotechnics, 71, 283–294. https://doi.org/10.1016/j.compgeo.2015.06.007

Damjanac, B., Detournay, C., & Cundall, P. (2020). Numerical Simulation of Hydraulically Driven Fractures. Modelling Rock Fracturing Processes: Theories, Methods, and Applications, 531–561.

Detournay, C., Damjanac, B., Torres, M., Cundall, P., Ligocki, L., & Gil, I. (2022). Heat Advection and Forced Convection in a Lattice Code–Implementation and Geothermal Applications. *Rock Mechanics Bulletin*, *1*(1), 100004.

Energy and Geoscience Institute at the University of Utah. (2024). Utah FORGE: Wells 16A(78)-32 and 16B(78)-32 Stimulation Pressure and Circulation Data April, 2024 [data set]. Retrieved from https://dx.doi.org/10.15121/2371032.

Fu, W, Savitski, A. A., Damjanac, B., & Bunger, A. P. (2019). Three-Dimensional Lattice Simulation of Hydraulic Fracture Interaction with Natural Fractures. Computers and Geotechnics, 107, 214–234. https://doi.org/10.1016/j.compgeo.2018.11.023

Fu, W., Damjanac, B., Radakovic-Guzina, Z., Finnila, A., Podgorney, R., & McLennan, J. (2024). Modeling Near-Wellbore Hydraulic Fracture Behaviors Under Combined Impacts of Wellbore Perforation and Natural Fractures. 58th U.S. Rock Mechanics/Geomechanics Symposium, Golden, Colorado, USA, ARMA-2024-1112.

Lee, Sang H., and Ahmad Ghassemi (2023). Modeling and Analysis of Stimulation and Fluid Flow in the Utah FORGE Reservoir. 48 th Workshop on Geothermal Reservoir Engineering Stanford University, Stanford, California, USA.

McLennan, J., England, K., Rose, P., Moore, J. & Barker, B. (2023). Stimulation of a High-Temperature Granitic Reservoir at the Utah FORGE Site. SPE Hydraulic Fracturing Technology Conference and Exhibition, The Woodlands, Texas, USA.

McClure, Mark, Garrett Fowler, Matteo Picone. (2022). Best Practices in DFIT interpretation: Comparative Analysis of 62 DFITs from Nine Different Shale Plays. SPE International Hydraulic Fracturing Technology Conference and Exhibition, Muscat, Oman.

McClure, M. (2023). Calibration Parameters Required to Match the Utah FORGE 16A (78)-32 stage 3 Stimulation with a Planar Fracturing Model. 48th Workshop on Geothermal Reservoir Engineering Stanford University, Stanford, California, USA.

Itasca. (2023). XSite — Hydraulic Fracture Simulation of 3D Fracture Networks (4.0).